



Development and Characterization of Fly Ash–BFS–Cement Composite for Engineering Applications

Harinandan Kumar¹ · Muralidhar Singh Munisingh²

Received: 12 June 2023 / Revised: 11 February 2024 / Accepted: 19 March 2024
© The Author(s), under exclusive licence to Chinese Society of Pavement Engineering 2024

Abstract

The paper deals with developing fly ash–Blast Furnace Slag (BFS) composite with additives like cement to utilize waste material in engineering applications. The additive-like cement with different proportions has gained particular attention worldwide because of the excellent bonding strength and enhancement of mechanical properties of fly ash composite with other admixtures. The geomechanical properties such as Unconfined Compressive Strength (UCS), Brazilian Tensile Strength (BTS), and California Bearing Ratio (CBR) of the developed composite at different curing periods (0, 7, 14, and 28 days) are reported in these studies. The optimum strength of the composite was determined at the maximum utilization of fly ash and BFS composite. The correlation among different strength parameters was established using the statistical approach. The composite with 80% fly ash, 12% BFS, and 8% cement showed the highest compressive strength. The results indicated an excellent bonding between the constituent materials of the composite with an adequate amount of strength. The strength parameters indicated the utilization of composite in haul road construction as a base or sub-base layer. Using composite will help the stable haul road and consume the bulk of fly ash and BFS to reduce environmental pollution.

Keywords Fly ash–BFS composite · Microstructural analysis · Mechanical properties · Statistical analysis

1 Introduction

A coal-based thermal power plant contributes 75% of the total thermal power plant because of coal availability. Nearly 120–150 MT/year of fly ash is produced from India's existing coal-fired thermal power plants [1, 2]. The dumped fly ash in the power plant's nearby area causes environmental and health hazards. Fly ash occupies an ample space of the fertile land if deposited outside. The dumping of fly ash not only acquires the land area but also reduces soil fertility [3]. Thus, using fly ash is a significant challenge to overcome the adverse environmental and human health effects. The engineering properties and the nature of fly ash to make a bond with admixture and filler materials make it suitable

for application in engineering and construction works. The increase in strength of the fly ash composite with admixture like lime, cement, NaOH, BFS, etc., has been observed by several researchers and reported elsewhere [4–6].

Like fly ash, blast furnace slag (BFS) is the waste material from steel plants and is usually dumped in nearby areas, causing environmental and human health hazards next to the fly ash. The utilization of BFS is also essential to reduce air and water pollution. The ash and BFS utilization percentages have not been encouraging despite many attempts.

Fly consists of a complex heterogeneous mixture of amorphous and crystalline phases of the constituting elements [7]. It is a finely powdered Ferro aluminosilicate with Al, Ca, Mg, Fe, Na, and Si as the main elements. The fly ash also contains heavy metals like As, Ba, Hg, Cr, Ni, V, Pb, Zn, and Se [8–10]. Fly ash particles are spherical and vary from 0.5 to 100 μm in size. Fly ash contains significant silicon dioxide (SiO_2) in amorphous and crystalline form. Amorphous is smooth and rounded, whereas crystalline is sharp. Thus, the presence of calcium oxide and silica helps fly ash to develop the bonding with admixture and enhances fly ash composites' strength.

✉ Harinandan Kumar
harinandankumar88@gmail.com

¹ Department of Petroleum Engineering and Earth Sciences, University of Petroleum and Energy Studies, Bidholi, Via Prem Nagar, Dehradun, Uttarakhand 248007, India

² Department of Mechanical Engineering, RV Institute of Technology and Management, Chaithanya Layout, 8th Phase, J. P. Nagar, Bengaluru, Karnataka 560076, India

India is the third-largest country in producing steel. Estimation indicates the production of 88.4 MT of steel in 2017 will increase up to 128.6 MT by 2021. About 70% of India's steel production is iron ore-based [11]. In the iron ore-based show, the ore is melted and reduced to pig iron in a blast furnace, which forms slag. The slag is about 30% pig iron [11]. Two types of blast furnace slags are produced during steel production: air-cooled slag and water-cooled slag [12]. Water-cooled blast furnace slag is generally utilized to produce slag cement, but air-cooled blast furnace slag is rarely used. Air-cooled blast furnace slag solidifies and crystallizes, creating a rock-like slag, with little or no cementing property that is why it is only used as coarse aggregate. Thus, the air-cooled blast furnace slag is the waste material from the steel plant and is usually dumped in nearby areas, causing environmental and human health hazards next to the fly ash. It harms the environment by polluting air and water. The utilization of BFS is another challenge to reduce environmental risks.

The bonding of fly ash with BFS and other admixtures makes the fly ash–BFS composite suitable for engineering works like road construction and civil works. A study was carried out to improve the mechanical strength of fly ash composite by adding nano-TiO₂ at variable composition from 0.4% to 2% [13]. An improvement in the mechanical strength of fly ash composite was reported with the addition of eggshell because of the additional bonding of the molecules [14]. The slag with red mud was used to develop a red mud-slag geopolymer (RM-SGP). The developed composite was found mechanically suitable for its application as a building products [15]. Ground granulated blast furnace slag (GGBFS), fly ash (FA), and cement mixture was used to develop a composite for engineering application. Results indicated acceptable shear strength of the composite at 50% cement, 25% FA, and 25% GGBFS [16]. Silica fume and crumb rubber were added to the fly ash–cement mixture to improve the mechanical properties of the composite. Results indicated the impact of silica fume in the improvement of the mechanical strength of the composite due to molecular solid bonding [17]. The filling material like cement in fly ash composite has gained particular attention worldwide because of the enhancement of bindings and compressive strength of composite [4, 6, 18–20]. The study was carried out to develop fly ash composite with alkali at variable particle sizes and percentages from 10% to 40% by weight. Different properties like tensile, flexural, and impact strength were experimentally determined, and observed an increase in tensile and flexural strengths with alkali material in fly ash composites [21]. The investigation was carried out to determine the compression strength of fly ash–cement composite samples with variations in the composite composition of admixture. The results indicated a higher load-carrying capacity of the composite at 4–8% of Portland cement and

10–20% of fly ash. The composite's compressive strength was increased with compaction and the curing period [22–24]. The geotechnical properties of untreated fly ash, fly ash–mine overburden mixes, and clinker-treated fly ash–mine overburden mixes were observed at variable compositions and reported that the strength parameters depend upon the percentage of fly ash and clinker in the composite. An increase in California Bearing Ratio (CBR) and unconfined compressive strength (UCS) was observed with the addition of the clinker [25, 26]. The increase in compressive strength of cement in fly ash–cement composite with a curing period from 7 to 58 days was reported elsewhere [27]. The investigation was carried out on fly ash–BFS–Cement composite at the variable composition of admixture and reported an increased compressive strength of the composite with 10% fly ash and 10% BFS [28].

The literature survey indicates the enhancement of the fly ash composite with BFS and other cementing materials. Therefore, the investigation was carried out to develop the fly ash–BFS composite with a variable percentage of cement to utilize these waste materials for engineering work and reduce its adverse effects on the environment and human health. This paper deals with the microstructural characterization of fly ash and BFS material and develops a composite with a mixture of fly ash, BFS, and cement at varying percentages. The developed composites were tested to determine mechanical strength like Unconfined Compressive Strength (UCS), Brazilian Tensile Strength (BTS), and California Bearing Ratio (CBR). The strength parameters were also determined for the samples with water cured for 7–28 days. The correlation between different percentage parameters and mechanical properties was established using the least square method. The strong influence of BFS and cement on strength parameters was observed. An increase in strength was observed with an increasing curing period, indicating the development of strong bonding in composite with time. The best composition of the material was obtained with the highest UCS, BTS, and CBR values.

The result of the study indicated an acceptable range of mechanical properties for its application as filler material in road construction. This paper's process and results are significant in utilizing the waste material as fly ash, BFS in bulk, and its engineering application.

2 Objectives

The study's objectives were to utilize the maximum amount of fly ash and BFS from the Coal-Fired Power Plant and Steel Plant by developing the fly ash–BFS composite with cement. The composites were formed to utilize fly ash and BFS in road construction, building construction, etc., to

enhance the mechanical properties. The objectives were achieved by following the methodology, as shown in Fig. 1.

2.1 Methodology

The methodology of the study is represented in Fig. 1. Samples of fly ash, BFS, and cement were collected from the study area and prepared to determine physical properties, followed by microstructural analysis. Based on the results of the physical and microstructural properties, the composition of the samples was decided to develop the composite material. The sample was molded in a cylindrical shape as per

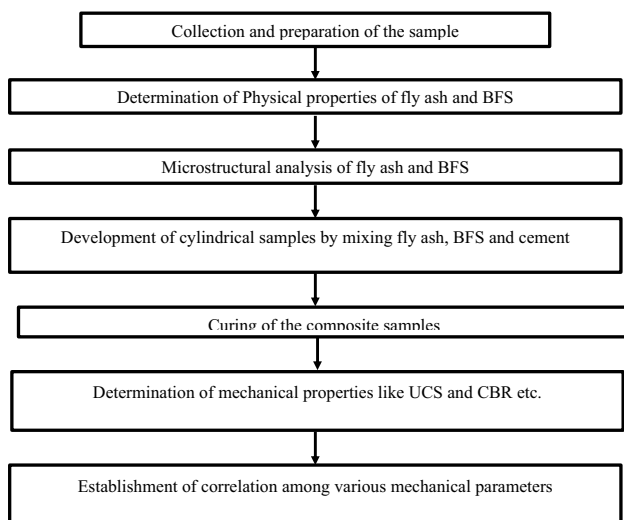


Fig. 1 Flow chat for development of fly ash–BFS composite, microstructural as well as mechanical properties characterization and optimization

the prescribed standard. The prepared samples were soaked with water and cured from 0 to 28 days. The samples were then tested to determine the geo-mechanical properties like unconfined compressive strength (UCS), Young’s modulus, Poisson’s ratio, etc. The results of testing the samples were mutually correlated to evaluate their engineering applicability. A similar approach has been suggested elsewhere [16, 17].

2.2 Samples Collection

Fly ash was collected from the hopper’s discharge channel in Rayalaseema Thermal Power Project (RTPP), Kadapa, Andhra Pradesh, India (Fig. 2a). Blast furnace slag (BFS) and Portland cement (53 grades) were collected from Garuda Steel Plant, Tadipathri, Anantapur, Andhra Pradesh, India, and the local market (Fig. 2b). The Fly ash, BFS, and cement were stored in plastic-covered jute bags to prevent ambient moisture. The collected samples were transported to the laboratory to develop a composite and determine microstructural and mechanical properties.

2.3 Samples Preparation

Composites were developed with collected fly ash, BFS, and cement material, as shown in Fig. 3a. The samples were prepared by mixing various proportions of fly ash, BFS, and cement materials, as represented in Table 1. The percentage was selected to utilize maximum fly ash and BFS. Powdered fly ash and BFS of size less than $75\ \mu$ were prepared for X-ray Diffraction (XRD) and Scanning Electron Microscope (SEM) analysis (Fig. 3b). The powdered fly ash and BFS samples were gold-coated to obtain a clear view of the SEM

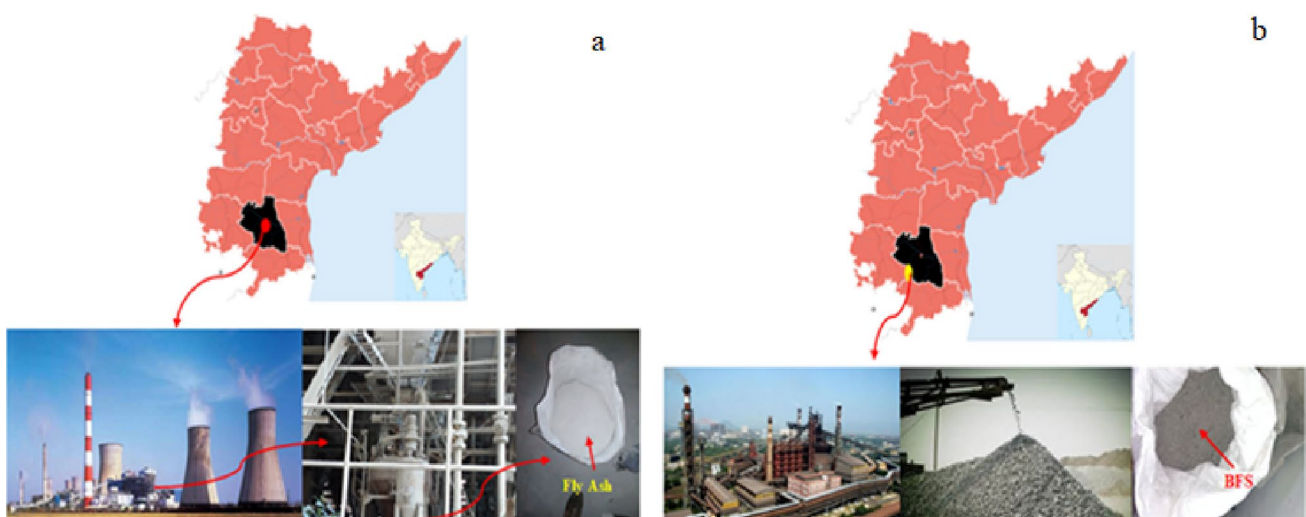


Fig. 2 Sample collected for analysis. **a** Fly ash sample collected from RTPP power plant, Andhra Pradesh. **b** BFS sample collected from Garuda Steel Plant, Andhra Pradesh

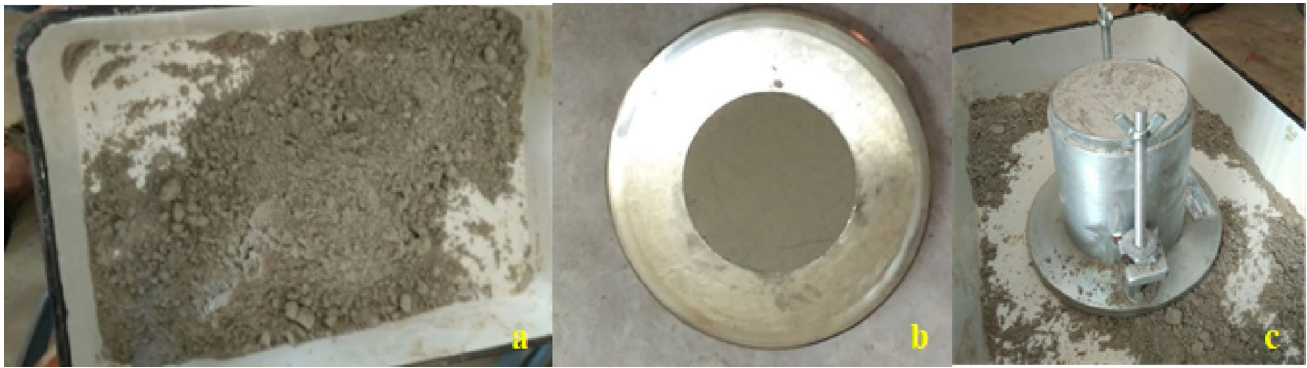


Fig. 3 Sample preparation for analysis. **a** Mixture of fly ash, BFS and cement for development of composite. **b** Sample prepared for microstructural analysis. **c** Mixture of fly ash, BFS and cement material in mould for compaction testing

Table 1 Percentage of fly ash, BFS and cement in composites

S. no	Sample id	Fly ash (%)	BFS (%)	Cement (%)
1	FA-BFS-C-1	80	12	8
2	FA-BFS-C-2	78	15	7
3	FA-BFS-C-3	76	18	6
4	FA-BFS-C-4	74	21	5

image. The optimum moisture content and maximum dry density of the fly ash, BFS, and cement material mixture were determined using a proctored test as per the standard [ASTM, UTS-0602] [29]. The split mold of 100 mm diameter and 152 mm length was used for the compaction test (Fig. 3c). Table 1. Percentage of fly ash, BFS and cement in composites.

Samples for unconfined compressive strength were prepared as per standard [IS 2720-Part 10 (1991)] [30]. The split mold of 38 mm diameter and 74 mm length was used to prepare the samples (Fig. 4a). A 36 mm diameter and 72 mm length size were obtained for the compressive strength test. The Brazilian tensile strength (BTS) test sample was prepared using the same mold of UCS test samples. The prepared specimen was made to maintain a length-to-diameter ratio of 0.5. Samples were prepared using a standard CBR mold of 100 mm diameter and 152 mm height (Fig. 4b) as per IS: 2720-Part 16 (1987) [31]. The sample was statically compacted in the mold, so that the height was maintained at 152 mm.



Fig. 4 Sample prepared for strength testing. **a** Sample for UCS test, **b** sample prepared for CBR test

Fig. 5 Microstructural analysis. **a** XRD analysis, **b** SEM and EDX analysis

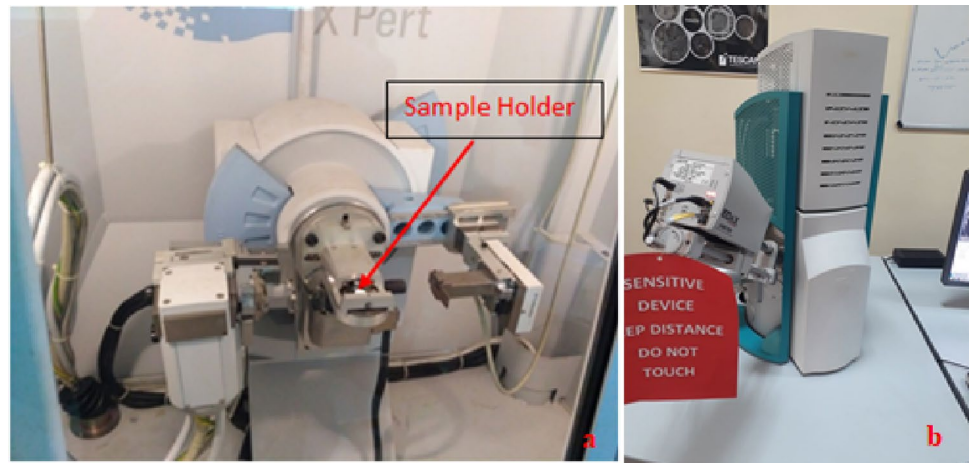


Table 2 Grain size distribution [34]

Classification of soils	Range of particle size
Gravel	> 4.75 mm
Sand	4.75–0.075 mm
Silt	0.075–0.002 mm
Clay	< 0.002 mm

3 Experimental Procedure

The testing procedures are crucial as the data obtained from the tests are considered for the developed composite characterization. Therefore, the standards testing approach was followed to determine the properties of developed composites.

3.1 Procedure Microstructural Analysis

The X-ray diffraction analysis of fly ash, BFS, and developed composite was carried out using Standard X-ray diffraction powder patterns. XRD analysis used a Philips diffractometer (Make: PANalytical X-ray B.V., UK) (Fig. 5). The SEM and

Energy Dispersive Spectroscopy (EDS) analyses were carried out to visualize the morphological characteristics of the composite.

3.2 Procedure for Determination of Physical and Mechanical Properties

The grain size distribution of fly ash and BFS was determined using a sieve set as per standard procedure IS 2720 Part 4 (1985) [32] (Table 2). The specific gravity of fly ash and BFS was determined by the pycnometer method as per standard [IS 2720-Part 3 (1980)] [33] (Fig. 6a).

Loss on ignition of fly ash and BFS were determined as per standard procedure in muffle furnaces as per IS 1760-Part 1 (1991) [35] (Fig. 6b). The sample's known weight was taken in the crucible and kept in the muffle furnace at 210 °C for 1 h. The crucible was then removed from the furnace, air-cooled for 10 min, and weighted to determine ignition loss. Consistency limits as the liquid limit (LL), plastic limit (PL), shrinkage limit, plasticity index (PI), and Free swell were determined as per standard procedure [IS 2720-Part 5 (1985) and Part 6 (1972)] [36, 37] (Fig. 6c). The specimen was compacted into the pre-weighted proctor mold by three

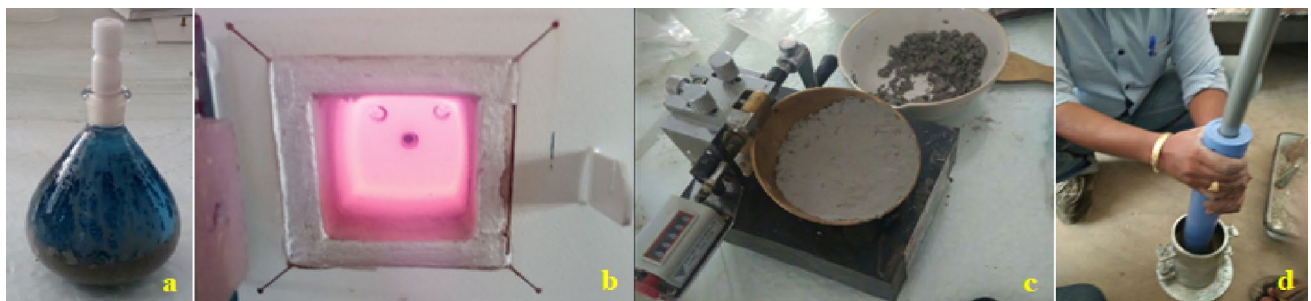


Fig. 6 Procedure to determine physical properties of the composite. **a** Determination of specific gravity, **b** determination of loss on ignition using muffle furnace, **c** determination of consistency limits, **d** compaction test

layers. The rammers weighing 2.5 kg were dropped from a height of 305 mm for better compaction (Fig. 6d). Samples were kept inside the mold in three layers and rammed for 25 blows for each segment. The collar of the mold was removed, and excess material was trimmed out. The mold, along with the sample, was weighed and recorded. A small quantity of samples was obtained to determine the moisture content by oven drying.

Unconfined compressive strength was determined as per standard procedure [IS 2720-Part 10 (1991)] [30] at a 1.2 mm/min strain rate. A similar approach was adopted elsewhere [38]. Unconfined compressive strength is a conventional method to determine its resistance to external loading. The samples prepared for the compressive strength test were kept between the frictionless bearing plates. A hardened steel ball was placed on the bearing plate. Adjust the specimen precisely to the centerline to apply the load uniformly. Axial and lateral deformation in the sample was detected using Linear Variable Differential Transformer (LVDT). The load was continuously applied in displacement mode to obtain the post-failure plot. The experimental setup for the unconfined compression test of the specimens is shown in Fig. 7a.

The direct tensile strength of fly ash composite is difficult, so indirect tensile strength or Brazilian tensile strength (BTS) was determined as per ASTM D3967 standard [39]. The Brazilian tensile test makes the sample fail under tension, though the loading pattern is compressive. In this test, the length-to-diameter ratio of the sample was taken at 0.5. The specimens prepared for the tensile strength test were 36 mm in diameter and 72 mm long. The specimens were placed diametrically during the test. The load is applied until the sample fails diametrically in tension (Fig. 7b). California

bearing ratio (CBR) was determined as per standard procedure [IS 2720-Part 16 (1987) [31]. The samples were statically compacted to 95% of maximum dry density in the CBR test mold. Two surcharge disks, each weighing 2.5 kg, were placed over the sample, and a plunger, 50 mm in diameter, was used to penetrate the sample at a rate of 1.25 mm/min during the CBR test (Fig. 7c).

3.3 Physical and Chemical Properties

The physical properties of fly ash and BFS are shown in Table 3. The specific gravity of fly ash and BFS obtained are 2.025 and 2.337. Less specific gravity was observed in fly ash compared to that of BFS due to higher iron and scrap metal content in BFS. The construction materials

Table 3 Physical properties of fly ash and BFS Material

Properties	Fly ash	BFS	Cement
Specific gravity	2.025	2.337	3.12
Particle size analysis (%)			
Gravel (> 4.75 mm)	4.2	15	–
Sand (4.75–0.075 mm)	45	55	–
Silt (0.075–0.002 mm)	29.2	18	–
Clay (< 0.002 mm)	21.6	12	–
Consistency limits			
Liquid limit (%)	25.165	33.34	–
Plastic limit (%)	7.236	0	–
Shrinkage limit (%)	–	–	–
Plasticity index (%)	17.928	–	–
Free swell index (%)	Negligible	Negligible	–
LOI	2.8	–	2.7

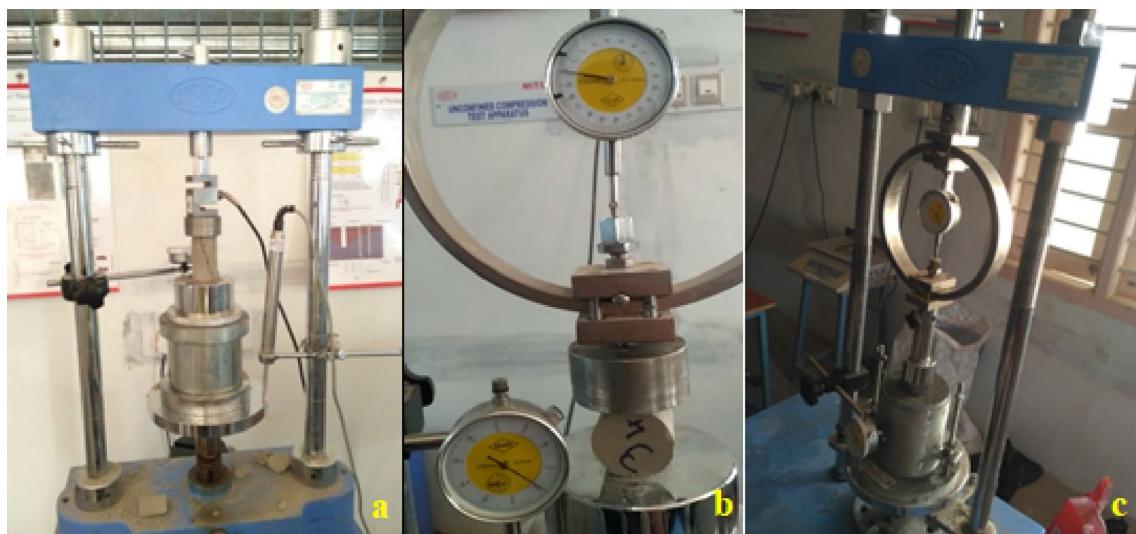


Fig. 7 Experimental setup for different testing **a** UCS test, **b** BTS test, **c** CBR test

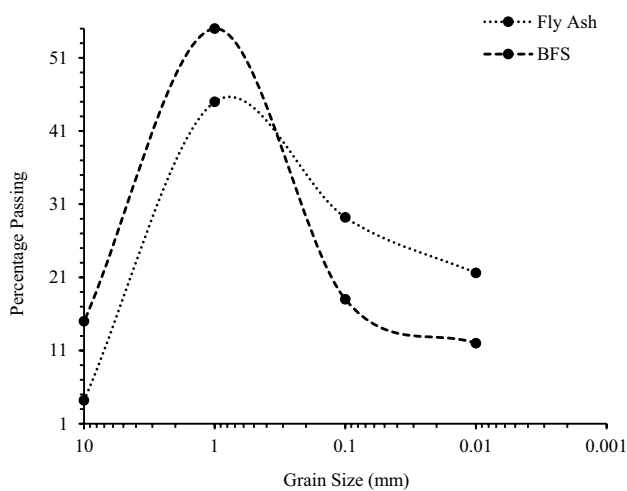


Fig. 8 Grain size distribution curves of fly ash and BFS

are susceptible to the density and grain size distribution. The smaller grain size leads to higher density and thus increases the strength of the composites. A similar observation has been reported elsewhere [40]. Therefore, the grain size distribution analysis was carried out, and the correlation was established between grain size distribution and the passing percentage of fly ash and BFS (Fig. 8). Various fly ash and BFS sizes were mixed in pre-determined proportions to develop the composites. Fly ash contains 4.2% gravel, 45% sand, 29.2% silt, and 21.6% clay particles.

Similarly, the BFS includes 15% gravel, 55% sand, 18% silt, and 12% clay particles. More than 50% of fly ash was observed from 20 to 75 μm . Therefore, the fly ash was categorized under non-plastic inorganic coarse silt-sized fractions. The material identification and classification are typically carried out using consistency limits such as the liquid limit (LL), plastic limit (PL), plasticity index (PI), and shrinkage limit. These parameters are essential to reflect the swelling potential and workability of the materials. The LL of fly ash and BFS were observed as 25.165 and 33.34, respectively. The higher value of the LL for BFS confirms the less workability of the fly ash than that of the BFS. The stabilization of the material depends upon the plasticity index of the stabilizing element. The plasticity index (PI) of fly ash was 17.928, while it was negligible for BFS. As the plasticity index (PI) of the cement is greater than 20% and capable of stabilizing any materials in the presence of water for hydration, it stabilizes the pozzolanic fly ash very fast. The non-cohesive and negligible shrinkage index of the fly ash and BFS confirm its suitability in geotechnical applications. The loss of ignition of fly ash was determined as 2.8%, which is lesser than the threshold value of 5–6%, confirming the suitability of fly ash to enhance the workability, durability, and mechanical properties of composite [41].

The important minerals identified in the fly ash and BFS were SiO_2 , Al_2O_3 , Fe_2O_3 , CaO , and MgO . These oxide compositions varied from 36.46% to 51.83%, 13.32% to 29.98%, 0.54% to 5.37%, 1.29% to 42.06%, and 0.52% to 7.59%, respectively, for fly ash as well as BFS materials (Table 4). The mineral identified in the FA and BFS samples was determined as major or minor phases depending on the intensity of the peaks, which indicates the quantity of the minerals present in the samples [42, 43]. The most abundant minerals observed in the FA were SiO_2 , Al_2O_3 , and Fe_2O_3 , but less CaO and MgO composition. The sum of silica, alumina, and iron contents was observed by more than 70%. Therefore, fly ash is classified as F type as per ASTM618-08a, 2008 [44], and confirms that the fly ash is produced by burning bituminous coal.

3.4 Microstructural Analysis

Fly ash was collected from the electrostatic precipitators (ESP) and tested for microstructural analysis using FESEM. Glassy solid spheres, hollow spheres (cenospheres), rounded and smooth porous grains, and irregular agglomerates were observed in SEM Images as represented in Fig. 9. Energy Dispersive Spectroscopy (EDS's) result in Fig. 9 confirms the predominant elements in the fly ash, such as silicon, aluminum, iron, calcium, and oxygen. The morphological and EDS analysis exhibited more than 50% amorphous alumino-silicate spheres, while the iron-rich spheres were significantly less. The presence of alumino-silicate spheres in various sizes confirms the possibility of packing material when used in the composites. The FESEM image indicated the rounded, sub-rounded, and sub-angular shape of the particles in the BFS material (Fig. 10). The sand to silt-size BFS particles had sub-rounded to angular shapes with rough surface texture. The result of EDS confirms the principal elements in the BFS as silicon, aluminum, magnesium, iron, calcium, and oxygen. The presence of sub-rounded to angular shapes of the particles in various sizes confirms its applicability in the composites. The FESEM image of the developed composite (80% FA + 12% BFS + 8% C) is shown in Fig. 11. The image exhibits the packing and bindings of the individual material with cement. The strong packing and bindings of the materials at seven days of curing confirm the enhancement of the composites' mechanical strength with curing.

Table 4 Mineral composition of the fly ash and BFS

	SiO_2	Al_2O_3	Fe_2O_3	CaO	MgO
FA	51.83	29.98	5.37	1.29	0.52
BFS	36.46	13.32	0.54	42.06	7.59
Cement	22.89	4.27	2.88	66.2	1.91

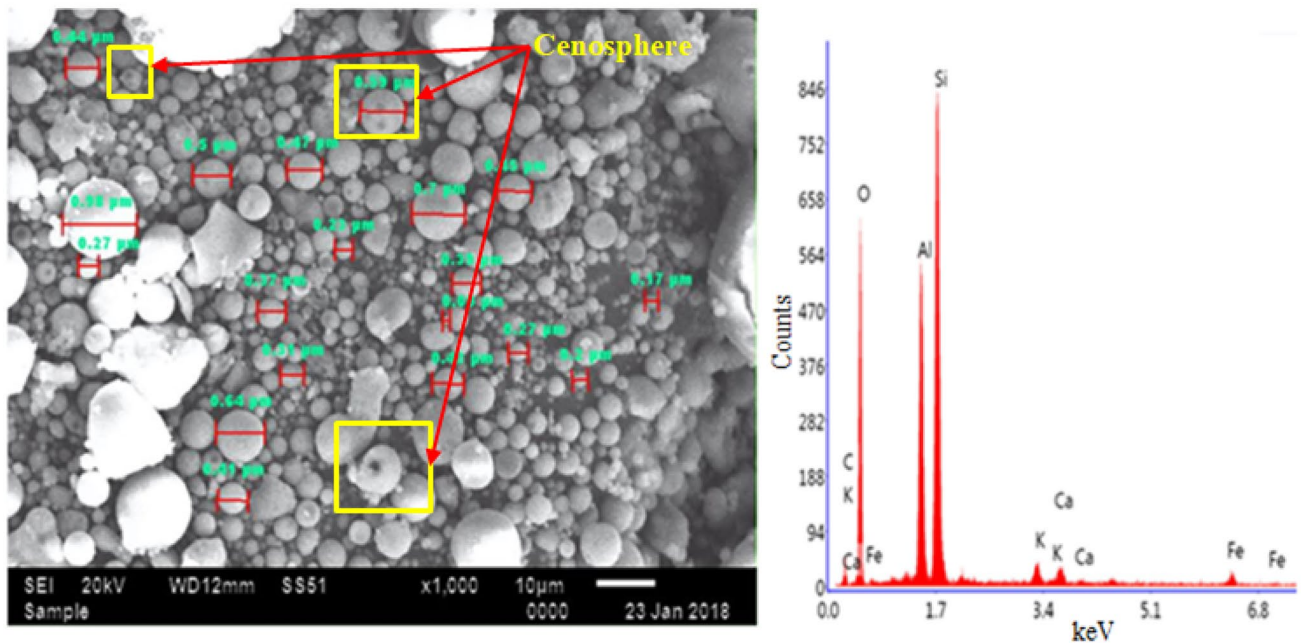


Fig. 9 FESEM images showing fly ash

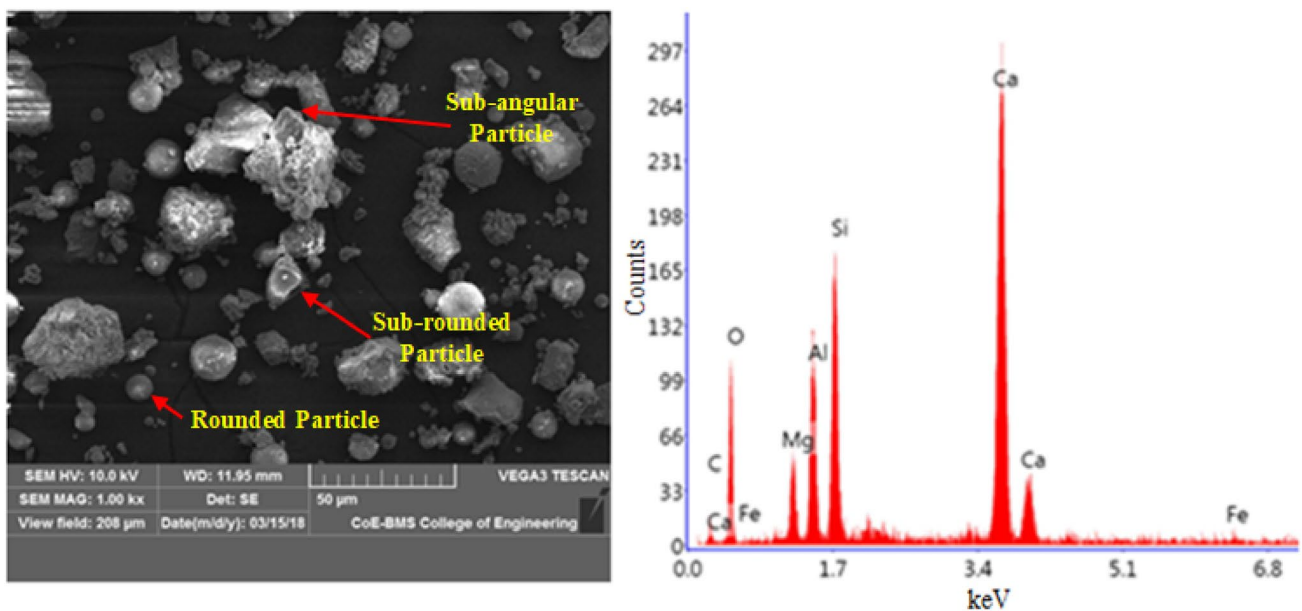


Fig. 10 FESEM images showing BFS

X-ray diffraction pattern of composite (80% FA + 12% BFS + 8% C) at 7 days curing exhibits the essential minerals of fly ash such as Augite, Silica, Quartz, and Mullite along with Calcite due to the presence of BFS (Fig. 12). The presence of Sillimanite peaks, an aluminosilicate compound, signifies the enhanced level of geo-polymerization. The composite's calcite peaks indicate the cross-linkage between the aluminum, silica, and calcium ions. In addition,

the higher percentage of calcium ions in BFS was responsible for the dissolution of the Si and Al ions. The presence of the hydration product and the increase in material volume due to the bonding of the undissolved solid particles into the geo-polymeric framework leads to the formation of the composites' dense structure. The composite's compact structure is responsible for the hardening of the whole system and enhancing the mechanical properties of composites.

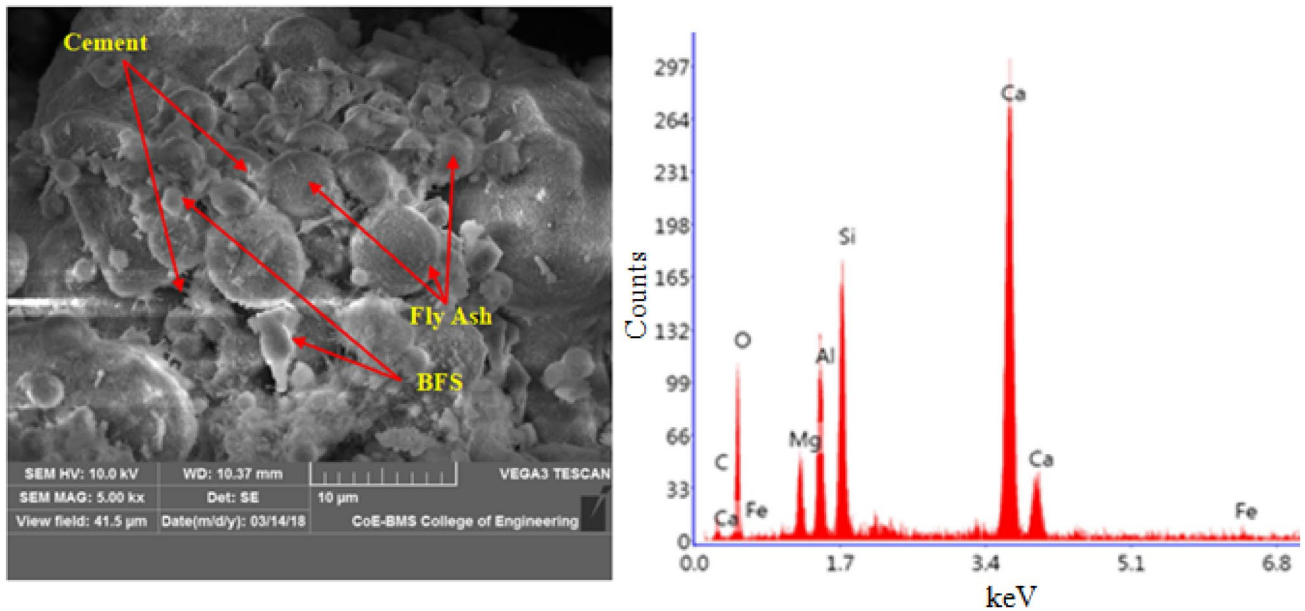


Fig. 11 FESEM images showing fly ash–BFS–cement composite at 7 days curing

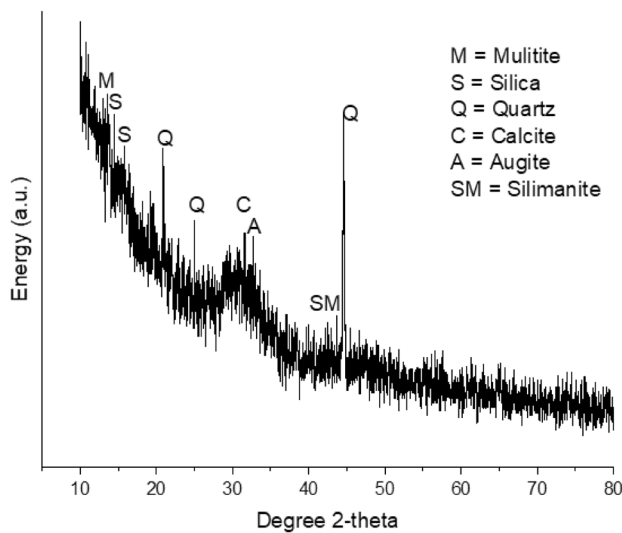


Fig. 12 XRD of fly ash–BFS–cement composite at 7 days curing

4 Results and Discussion

The research's objective was to utilize the maximum amount of hazardous fly ash and BFS as waste materials for the power plant and steel plants. The aim is achieved by developing and testing the fly ash–BFS composites for their mechanical strength at different curing periods. The results of the investigation have been discussed in the following sub-sections.

4.1 Mechanical Properties

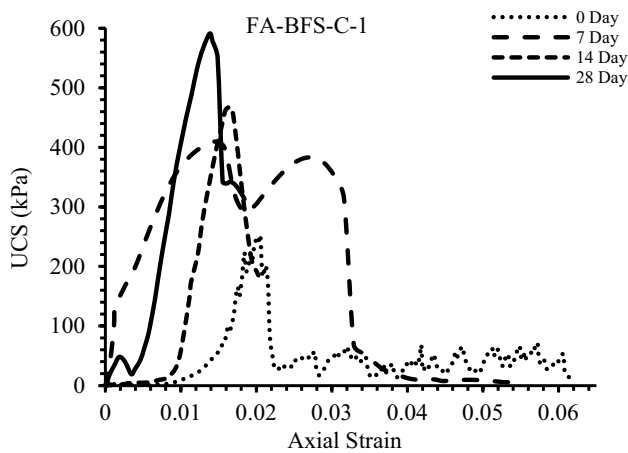
The compression test typically determines the construction materials' ability, like fly ash composites, to withstand the load when it is compressed. Those composites' compressive strength reveals the constituent elements' behavior under the compressive load. The different compressive testing [Uniaxial compressive strength (UCS), Brazilian tensile strength (BTS), and California bearing ratio (CBR)] were carried out to determine the strength parameters of the developed composites. The testing was carried out per the standard described in the experimental procedure. The results of the testing are presented in the following sub-sections.

4.1.1 Uniaxial Compressive Strength (UCS)

The cylindrical specimens of the developed composites representing different compositions were examined to determine the compressive strength. The compressive strength of both uncured and cured samples is discussed here. The average values of the twenty best samples' mechanical properties representing each composite are shown in Table 5. In the uniaxial compression tests, the stress–strain curve was developed for each specimen to determine coal strength, elastic modulus (Young's modulus of elasticity), and Poisson's ratio (Fig. 13). The stress–strain curve's maximum stress or peak load represents uniaxial compressive strength. Young's modulus is the slope of the stress–strain curve in the linear elastic (loading) stage. Poisson's ratio was determined at the linear elastic (loading) stage. Figure 14 represents the

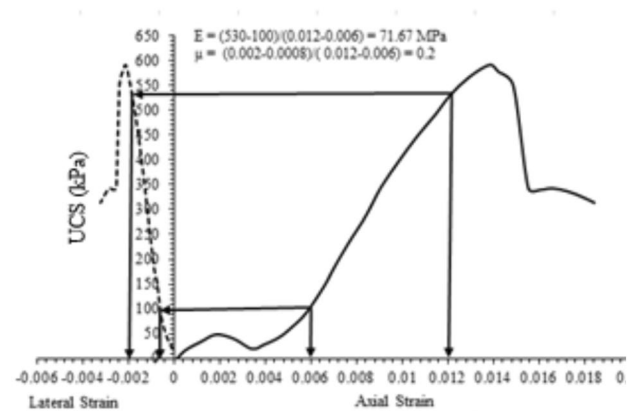
Table 5 Mechanical properties of the composites

S. no	Sample id	Composition	Curing period (days)	Compressive strength (kPa)	Poisson's ratio (μ)	Young's modulus, E (MPa)
1	FA-BFS-C-1	80% FA + 12% BFS + 8% C	0	252.63	0.20	27.27
2			7	409.81	0.25	28.73
3			14	465.73	0.26	48.21
4			28	591.09	0.28	71.67
5	FA-BFS-C-2	78% FA + 15% BFS + 7% C	0	203.45	0.26	36.99
6			7	214.96	0.19	40.55
7			14	380.88	0.18	79.35
8			28	417.90	0.16	92.86
9	FA-BFS-C-3	76% FA + 18% BFS + 6% C	0	62.67	0.24	15.67
10			7	86.69	0.27	18.98
11			14	94.49	0.3	19.89
12			28	100.17	0.2	20.86
13	FA-BFS-C-4	74% FA + 21% BFS + 5% C	0	205.35	0.31	11.51
14			7	270.35	0.34	29.49
15			14	353.88	0.34	69.61
16			28	635.73	0.29	119.30

**Fig. 13** Variation of strength of developed composites with curing

model to determine Young's modulus and Poisson's ratio of all composite.

The stress-strain plot reveals the almost linear-elastic behavior of the composites before yielding or failure. Each specimen exhibits brittle behavior with minimal plastic deformation. The compressive strength was also determined for each composite at different curing periods, varying from 0 to 28 days. The composite FA-BFS-C-1 exhibited higher UCS, i.e., 252.63 kPa, while composite FA-BFS-C-3 exhibited lower UCS at 62.67 kPa at 0 days curing (Table 5). The UCS was nearly equal for the composite FA-BFS-C-2 and FA-BFS-C-4, i.e., 203.45 and 205.35 kPa, respectively, at 0 days curing (Table 5). THE highest UCS in FA-BFS-C-1 is due to the pozzolanic reaction of fly ash and BFS activated

**Fig. 14** Elastic modulus (E) and Poisson's ratio (μ) of composite FA-BFS-C-1 at 28 days curing

by the hydration products of Portland cement. A similar observation was carried out on the Portland cement-limestone powder-BFS composite and observed pozzolanic reaction between limestone powders and BFS in Portland cement reported elsewhere [45, 46].

The performance of different composites at varying curing periods from 0 to 28 days was analyzed and illustrated in Figs. 13 and 15a-c. It is observed that the compressive strength of all compositions increased with an increase in the curing period. The compressive strength of composites was smaller at the early stages of the curing period but increased gradually with the curing period due to the formation of hydration products and filling of the pores in the composite matrix. The UCS values of all composites at

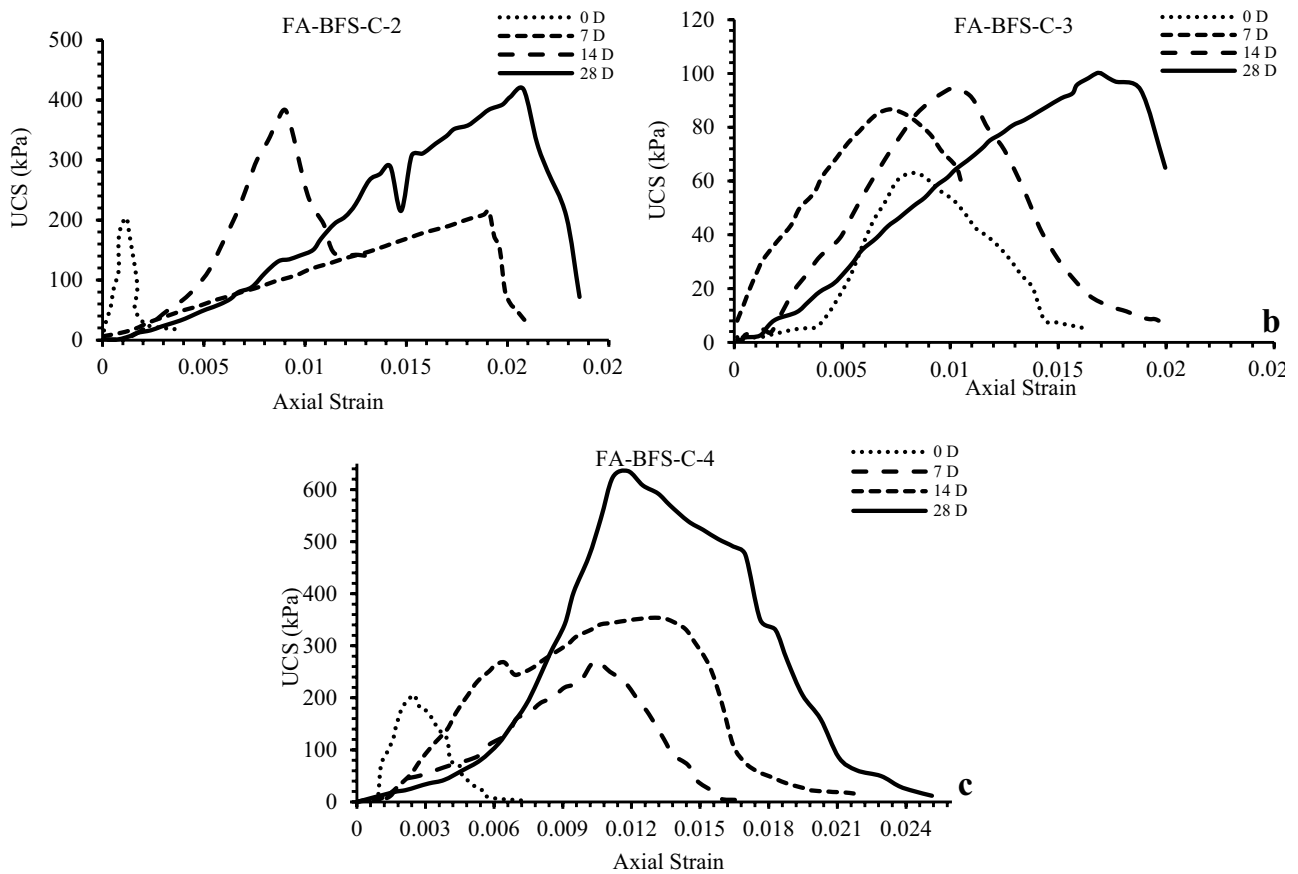


Fig. 15 Variation of strength of developed composites with curing. **a** Composite FA–BFS–C-2, **b** composite FA–BFS–C-3, **c** composite FA–BFS–C-4

7 days of curing exhibited from 86.69 to 409.81 kPa. The strength values were observed maximum for the sample with 80% FA, 12% BFS, and 8% C (Figs. 13 and 15a–c). The first drop in strength was observed at 282.52 kPa in the stress–stress curve of composite FA–BFS–C-1, exhibiting the first cracking developed in the composite during the compression (Fig. 13). The maximum strength of the composite FA–BFS–C-1 is due to the hydration reaction between pozzolanic FA and BFS and bonding material like cement in water that enhances the bonding between constituting materials of the composite. The composites' compressive strength at 14 and 28 days of curing exhibited 94.49–465.73 kPa and 100.17–635.73 kPa, respectively (Table 5). An increase in compressive strength was observed with the curing period (Figs. 13 and 15a–c). Compressive strength development in the composites with the curing period is attributed to the formation of hydration reaction products such as calcium silicate hydrate, calcium aluminate hydrates, etc. The fly ash in the composite enhances the hydration through the filler effect, thus improving the particles' packing and the formation of calcium silicate phases. The hydrous silica and alumina of fly ash gradually react with the calcium ions from

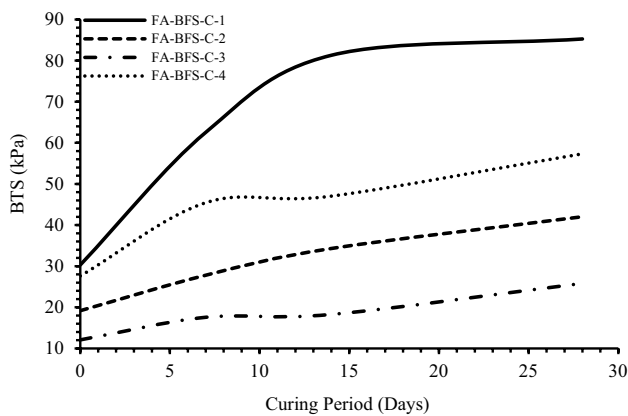
the hydration of cement and BFS to form insoluble calcium silicate and aluminate hydrate compounds [47]. Hydrated compounds' formation increases the specific volume and fills the open pores of the matrix in the composite. The filling of the pores in the matrix makes the structure denser and enhances the composite's strength. Similar observations have been carried out and improved compressive strength with the curing period reported elsewhere [47, 48]. The decreased compressive strength of composite FA–BFS–C-3 compared to others was attributed to the hindrance infilling of the matrix's pores.

4.1.2 Brazilian Tensile Strength (BTS)

The indirect tensile strength was determined to evaluate the strength properties of the developed composites. The average of five best values of BTS of each composition is represented in Table 6. The BTS varies from 12.10 to 30.33 kPa, 17.59 to 62.58 kPa, 18.27 to 81.30 kPa, and 25.84 to 85.27 kPa during periods 0, 7, 14, and 28 days respectively (Table 6). An increase in BTS with a curing period was observed in all composites (Fig. 16). The composite

Table 6 Results of BTS of the developed composites

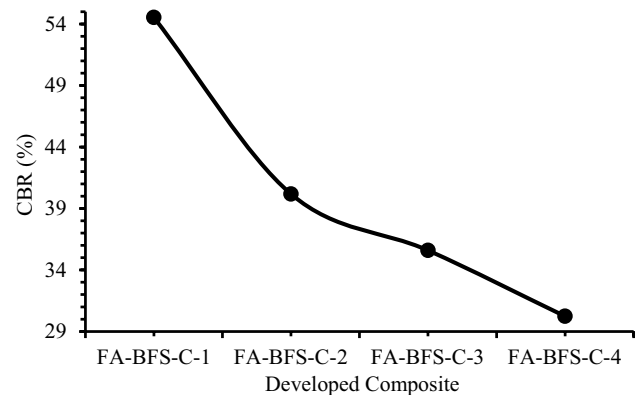
S. no	Sample id	Composition	Curing period (days)	Brazilian tensile strength (kPa)
1	FA-BFS-C-1	80% FA + 12% BFS + 8% C	0	30.33
2			7	62.58
3			14	81.30
4			28	85.27
5	FA-BFS-C-2	78% FA + 15% BFS + 7% C	0	19.18
6			7	27.81
7			14	34.33
8			28	42.04
9	FA-BFS-C-3	76% FA + 18% BFS + 6% C	0	12.10
10			7	17.59
11			14	18.27
12			28	25.84
13	FA-BFS-C-4	74% FA + 21% BFS + 5% C	0	27.63
14			7	45.45
15			14	47.05
16			28	57.36

**Fig. 16** Variation of tensile strength of composites with curing periods

with 80% FA + 12% BFS + 8% C exhibited maximum tensile strength compared to others at 7, 14, and 28 days of curing, respectively (Fig. 16). The higher tensile strength of the composite FA-BFS-C-1 is due to the pozzolanic reaction of fly ash and BFS. The strength is due to the presence of cement and adequate water to form hydration products like calcium silicate hydrate, calcium aluminate hydrates, etc. Thus, the tensile strength was observed as a function of the developed hydration products, which increased with the curing period.

4.1.3 California Bearing Ratio (CBR)

California Bearing Ratio exhibits the index of strength and bearing capacity of the composites. Therefore, the CBR

**Fig. 17** Variation of CBR percentage with composites

percentage was determined to characterize the un-cured FA-BFS composite's strength and bearing capacity. The variation of the CBR percentage of different composites is represented in Fig. 17.

A maximum CBR percentage was observed for composite FA-BFS-C-1. CBR percentage varies from 30.24% to 54.54%, with fly ash from 74% to 80%, respectively (Fig. 18). The FA-BFS-C-1 composite exhibited a CBR value of more than 50%, therefore considered excellent for sub-grade road pavement as recommended elsewhere [49]. The increase in CBR percentage with fly ash is due to silica and alumina in the fly ash that gradually reacts with the calcium ions of cement and BFS. The reaction formed insoluble calcium silicate and aluminate hydrate compounds and thus enhanced the composites' strength and bearing capacity. A similar observation was carried out for soil with class C

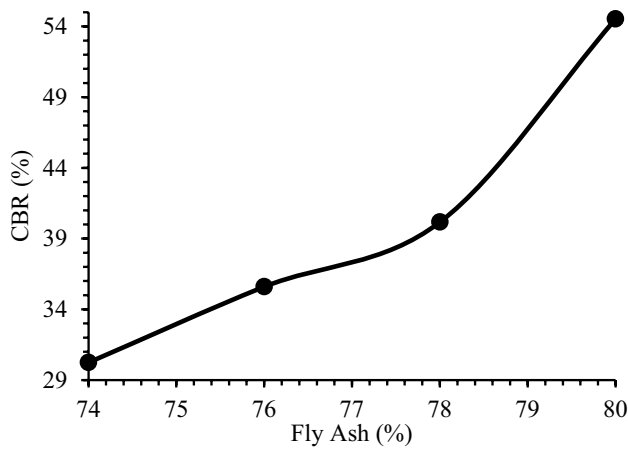


Fig. 18 Variation of CBR percentage with fly ash composition

Table 7 Calculated resilient modulus of the composite

S. no	Sample id	Composition	M_R (MPa)
1	FA–BFS–C-1	80% FA + 12% BFS + 8% C	227.52
2	FA–BFS–C-2	78% FA + 15% BFS + 7% C	187.10
3	FA–BFS–C-3	76% FA + 18% BFS + 6% C	173.16
4	FA–BFS–C-4	74% FA + 21% BFS + 5% C	155.99

fly ash, and an increased CBR percentage with fly ash was reported elsewhere [50].

4.1.4 Resilient Modulus (MR)

The resilient modulus (MR) is the elastic unloading modulus obtained after cyclic loading. It measures material stiffness and provides a means to analyze materials' stiffness under different stress levels. It is also a required input parameter to the mechanistic-empirical pavement design method. It is typically determined through laboratory tests by measuring a cylinder specimen's stiffness subject to a cyclic axle load. It is calculated as the ratio of applied axle deviator stress and recoverable axle strain [51]. In this investigation, the MR was determined based on CBR percentage using established correlations as per AASHTO T193, 2013 [52]:

$$M_R = 17.6(\text{CBR})^{0.64}$$

where M_R = Resilient Modulus (MPa), CBR = California Bearing Ratio (%).

The calculated Resilient Modulus is represented in Table 7. The maximum Resilience Modulus value of 227.52 MPa was observed for the composite FA–BFS–C-1, indicating an increase in stiffness of the composite with the addition of fly ash.

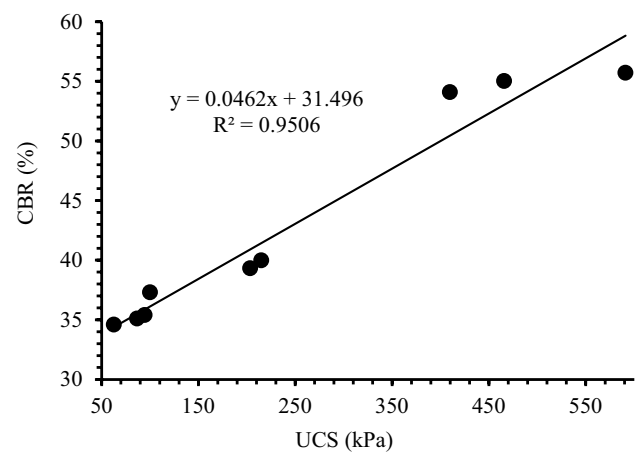


Fig. 19 Correlation of CBR percentage with compressive strength of composites

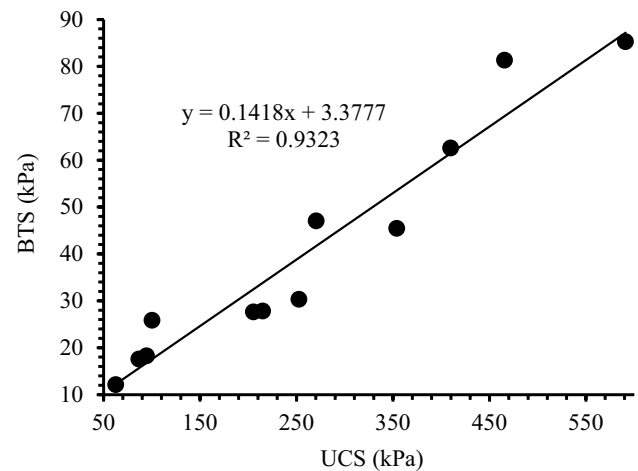


Fig. 20 Correlation of BTS with compressive strength of composites

4.2 Correlation of Tensile Strength and Bearing Ratio with Compressive Strength of Composites

The mutual correlation between tensile strength and the bearing ratio was established with the composite's unconfined compressive strength using the statistical approach, as represented in Figs. 19 and 20. The least-square linear regression method was considered to analyze the correlation between the above parameters. Linear correlations with a coefficient (R^2) of 0.95 were observed between the CBR percentage and UCS of all composites.

The strong linear correlation between BTS and UCS with R^2 0.93 confirms the relationship between tensile strength and the developed composites' compressive strength.

5 Conclusions

- The conclusions drawn from the investigations are summarized as follows:
- The physical properties exhibited the suitability of the developed composites for geotechnical applications.
- The presence of free lime (CaO) and free magnesia (MgO) in the constituent materials indicates the stabilization of materials in composites.
- The FESEM analysis of the microstructure of fly ash exhibited glassy solid spheres, hollow spheres (cenospheres), rounded and smooth porous grains, and irregular agglomerates. The SEM study confirms the possibility of packing material when used in the composites.
- The strong packing and bindings of the materials at 7 days of curing confirm the enhancement of the composites' mechanical strength with curing.
- The XRD analysis indicated hydration products such as Augite, Silica, Quartz, Mullite, and Silimanite in the developed composite. The presence of the hydration product and increase in material volume due to the bonding of the undissolved solid particles leads to dense structure, hardening effect, and enhancement of mechanical properties of the composites.
- The stress–strain plot of the composites in UCS testing reveals the composites' almost linear–elastic behavior before yielding or failure. Each specimen exhibits brittle behavior with minimal plastic deformation. The increased compressive strength of all composites was observed with an increase in the curing period.
- An increase in BTS with a curing period was observed in all composites.
- CBR values of more than 50% were observed for composite FA–BFS–C-1, exhibiting combined suitability for sub-grade road pavement.
- The maximum Resilience Modulus value of 227.52 MPa was found for the composite FA–BFS–C-1, indicating an increase in the composite's stiffness with the addition of fly ash.
- A strong linear correlation was observed between CBR, BTS, and UCS was observed.

Author Contributions All authors of this research paper have directly participated in the planning, execution, or analysis of this study.

Funding No funding was obtained for this study.

Data availability The data used in the research work has been presented in the manuscript.

Declarations

Conflict of Interest On behalf of all authors, the corresponding author states that there is no conflict of interest.

References

1. Lokeshappa, B., & Dikshit, A. K. (2011). Single step extractions of metals in coal fly ash. *Materials and Structures*, 2, 01–08.
2. International Energy Agency. (2016). *Energy and air pollution*. World energy outlook special report.
3. Yuan, C. C., Fang, W. C., Mui, D. T., & Chiang, H. L. (2009). Application of methods (sequential extraction procedures and high-pressure digestion method) to fly ash particles to determine the elements a case study of BCR 176. *Journal of Hazardous Materials*, 163, 578–587.
4. Gorhan, G., & Kurklu, G. (2014). The influence of the NaOH solution on the properties of the fly ash-based geopolymer mortar cured at different temperatures. *Composites, Part B: Engineering*, 58, 371–377.
5. Kavitha, O. R., & Nandhinipriya, K. C. (2017). Effect of bottom ash as a mineral admixture in concrete. *Journal of King Saud University Engineering Sciences*, 10, 134–139.
6. Karthik, A., Sudalaimani, K., Vijayakumar, C.T. (2017). Durability study on coal fly ash-blast furnace slag geopolymer concretes with bio-additives. *Ceramics International*, 43, 11935–11943.
7. Leemann, A., Shi, Z., & Lindgard, J. (2020). Characterization of amorphous and crystalline ASR products formed in concrete aggregates. *Cement and Concrete Research*, 131, 105913.
8. Adriano, D. C., Page, A. L., Elseewi, A. A., Chang, A. C., & Straughan, I. (1980). Utilization and disposal of fly ash and other coal residues in terrestrial ecosystems: a review 1. *Journal of Environmental Quality*, 9, 333–344.
9. Aitken, R. L., & Bell, L. C. (1985). Plant uptake and phytotoxicity of boron in Australian fly ashes. *Plant and Soil*, 84, 245–257.
10. Mattigod, S. V., Rai, D., Eary, L. E., & Ainsworth, C. C. (1990). Geochemical factors controlling the mobilization of inorganic constituents from fossil fuel combustion residues: I. Review of the major elements. *Journal of environmental quality*, 19, 188–201.
11. Jain, V., Umesh, B. R., Venugopal, V. W., & Pradip, T. (2013). Processing of alumina-rich iron ore slimes: Is the selective dispersion–flocculation–flotation the solution we are looking for the challenging problem facing the Indian iron and steel industry. *Transactions of the Indian Institute of Metals*, 66, 447–456.
12. Giergiczny, Z. (2020). Fly ash and slag. *Cement and Concrete Research*, 124, 105826.
13. Ghanim, A. A. J., Amin, M., Zeyad, A. M., Tayeh, B. A., & Agwa, I. S. (2023). Effect of modified nano-titanium and fly ash on ultra-high-performance concrete properties. *Structural Concrete*, 1, 1464–4177.
14. Hakeem, I. Y., Abd-Al Ftah, R. O., Tayeh, B. A., & Hafez, R. D. A. (2023). Eggshell as a fine aggregate replacer with silica fume and fly ash addition in concrete: A sustainable approach. *Case Studies in Construction Materials*, 18, e01842.
15. Qaidi, S. M. A., Tayeh, B. A., Isleem, H. F., de Azevedo, A. R. G., Ahmed, H. U., & Emad, W. (2022). Sustainable utilization of red mud waste (bauxite residue) and slag for the production of geopolymer composites: A review. *Case Studies in Construction Materials*, 16, e00994.
16. Elsayed, M., Tayeh, B. A., Aisheh, Y. I. A., El-Nasser, N. A., & Elmaaty, M. A. (2022). Shear strength of eco-friendly self-compacting concrete beams containing ground granulated blast furnace slag and fly ash as cement replacement. *Case Studies in Construction Materials*, 17, e01354.
17. Alaloul, W. S., Musarat, M. A., Haruna, S., Law, K., Tayeh, B. A., Rafiq, W., & Saba Ayub, S. (2021). Mechanical properties of silica fume modified high-volume fly ash rubberized self-compacting concrete. *Sustainability*, 13, 5571.
18. Alahrache, S., Winnefeld, F., Champenois, J. B., Hesselbarth, F., & Lothenbach, B. (2016). Chemical activation of hybrid

- binders based on siliceous fly ash and Portland cement. *Cement and Concrete Composites*, 66, 10–23.
19. Li, C., Hao, Y. F., & Zhao, F. Q. (2018). Preparation of fly ash-granulated blast furnace slag-carbide slag binder and application in total tailings paste backfill. *IOP Conference Series, Materials Science and Engineering*, 322, 4–8.
 20. Pimraksa, K., Chindaprasirt, P., Sanjayana, J., & Ling, T. C. (2018). Alternative cementitious materials and their composites. *Advances in Materials Science and Engineering*, 2018, 1–2.
 21. Barnard, R. (2014). *Mechanical properties of fly ash/slag based geopolymer concrete with the addition of macro fibres*. Dissertation, Stellenbosch University.
 22. Yazici, H., Aydin, S., Yigiter, H., & Baradan, B. (2005). Effect of steam curing on class C high-volume fly ash concrete mixtures. *Cement and Concrete Research*, 35, 1122–1127.
 23. Rupnow, T. D., Wang, K., Schaefer, V., & Tikalsky, P. (2010). A simple method for characterizing and predicting temperature behavior of ternary cementitious systems. *Journal of Construction and Building Materials*, 25, 2290–2297.
 24. Alghazali, H., Aljazeera, R., & Myers, J. J. (2020). Effect of accelerated curing regimes on high volume fly ash mixtures in precast manufacturing plants. *Cement and Concrete Research*, 137, 106190.
 25. Behera, B., & Mishra, M. K. (2012). Strength assessment and compositional analysis of lime stabilized fly ash and mine overburden mixes upon curing. *The Journal of Solid Waste Technology and Management*, 38, 211–221.
 26. Mallick, S. R., Mishra, M.K. (2013). Geotechnical characterization of clinker-stabilized fly Ash - coal mine overburden mixes for subbase of mine haul road. *Coal Combustion and Gasification Products*, 5, 51–56.
 27. Alvin, H., Srivastava, V., & Herbent, A. (2014). Effect of fly-ash on compressive strength of Portland Pozzolona cement concrete. *Journal of Academia and Industrial Research*, 2, 2278–5213.
 28. Kalla, P., Misra, A., Gupta, R. C., Csetenyi, L., Gahlot, V., & Arora, A. (2013). Mechanical and durability studies on concrete containing wollastonite–fly ash combination. *Construction and Building Materials*, 40, 1142–1150.
 29. ASTM, UTS-0602 (2020) Soil Compaction Testing Equipment, ASTM International 100 Barr Harbor Drive, PO Box C700, West Conshohocken, PA 19428-2959. United States.
 30. IS 2720-Part 10 (1991) Methods of test for soils part 10: Determination of unconfined compressive strength, Second Revision, Bureau of Indian standards, Manak Bhavan, 9 Bahadur Shah Zafar Marg, New Delhi India.
 31. IS 2720-Part 16 (1987) Methods of test for soil part 16: Laboratory determination of CBR, Manak Bhavan, 9 Bahadur Shah Zafar Marg, New Delhi India.
 32. IS 2720-Part 4 (1985) Methods of test for soils part 4: Grain size analysis, Bureau of Indian standards, Manak Bhavan, 9 Bahadur Shah Zafar Marg, New Delhi India.
 33. IS 2720-Part 3 (1980) Methods of test for soils part 3: Determination of specific gravity, Bureau of Indian standards, Manak Bhavan, 9 Bahadur Shah Zafar Marg, New Delhi India.
 34. Behera, B. (2012). *Experimental and numerical investigation into behaviour of fly ash composite material in the subbase of surface coal mine haul road*. PhD thesis, NIT Rourkela.
 35. IS 1760-Part 1 (1991) Methods of chemical analysis of limestone, dolomite and allied materials, Part 1: Determination of loss on ignition, Manak Bhavan, 9 Bahadur Shah Zafar Marg, New Delhi India.
 36. IS 2720-Part 5 (1985) Method of test for soils part 5: Determination of liquid and plastic limit, Manak Bhavan, 9 Bahadur Shah Zafar Marg, New Delhi India.
 37. IS 2720-Part 6 (1972) Methods of test for soils part 6: Determination of shrinkage factors, Manak Bhavan, 9 Bahadur Shah Zafar Marg, New Delhi India.
 38. Chethan, B. A., & Shankar, A. U. R. (2023). Effect of flash flood and weather changes on unconfined compressive strength of cement- and fly ash-stabilized black cotton soil used as road materials. *International Journal of Pavement Research and Technology*, 16, 195–211.
 39. ASTM D3967 – 23 (2023) Standard Test Method for Splitting Tensile Strength of Intact Rock Core Specimens with Flat Loading Platens, ASTM International, 100 Barr Harbor Drive, PO Box C700, West Conshohocken, PA 19428-2959. United States.
 40. Marathe, S., Mithanthaya, I. R., Mithun, B. M., Shetty, S., & Akarsh, P. K. (2020). Performance of slag-fly ash based alkali activated concrete for paver applications utilizing powdered waste glass as a binding ingredient. *International Journal of Pavement Research and Technology*, 14, 196–203.
 41. Mehta, P. K., & Monteiro, P. J. (2017). *Concrete microstructure, properties and materials* (4th ed., Vol. 1, p. 142). McGraw Hill Education.
 42. Yildirim, I. Z., & Prezzi, M. (2011). Chemical, mineralogical, and morphological properties of steel slag. *Advances in Civil Engineering*, 2011, 254–260.
 43. Tikalsky, P. J., Roy, D., Scheetz, B., & Krize, T. (2002). Redefining cement characteristics for sulfate-resistant Portland cement. *Cement and concrete research*, 32, 1239–1246.
 44. C618 – 08a (2008) Standard Specification for Coal Fly Ash and Raw or Calcined Natural Pozzolan for Use in Concrete, ASTM International, 100 Barr Harbor Drive, PO Box C700, West Conshohocken, PA 19428-2959. United States.
 45. Zhou, J., Qian, S., Beltran, M. G. S., Ye, G., Breugel, K. V., & Li, V. C. (2010). Development of engineered cementitious composites with limestone powder and blast furnace slag. *Materials and Structures*, 43, 803–814.
 46. Shi, Z., & Lothenbach, B. (2019). The role of calcium on the formation of alkali–silica reaction products. *Cement and Concrete Research*, 126, 105898.
 47. Garga, M., & Pundi, A. (2015). Development of fly ash-based composite binder and its application in construction materials. *European Journal of Environmental and Civil Engineering*, 19, 1253–1267.
 48. Morsy, M. S., Alsayed, S. H., & Salloum, Y. A. (2012). Development of eco-friendly binder using metakaolin–fly ash–lime-anhydrous gypsum. *Construction and Building Materials*, 35, 772–777.
 49. Bowles, J. (1992). *Engineering properties of soil and their measurements* (4th ed.). McGraw-Hill.
 50. Ismaiel, H. A. H. (2006). *Treatment and improvement of the geotechnical properties of different soft fine-grained soils using chemical stabilization*. Ph.D. thesis, Martin Luther University Halle Wittenberg, Minnesota.
 51. MnDOT. (2018). Schedule of materials control. Standard Specifications, 1, 1–76.
 52. AASHTO: T 193-99 (2003) Standard Method of Test for The California Bearing Ratio, American Association of State and Highway Transportation Officials.

Springer Nature or its licensor (e.g. a society or other partner) holds exclusive rights to this article under a publishing agreement with the author(s) or other rightsholder(s); author self-archiving of the accepted manuscript version of this article is solely governed by the terms of such publishing agreement and applicable law.

Harinandan Kumar has completed his Ph.D. on the topic related to Geotechnical analysis of soft rock. He is a passionate researcher interested in the geomechanical behavior of rock and soil, unconventional reservoirs, the mechanical behavior of materials, and more. He has published over thirty research papers in international journals indexed by SCI, SCIE, and Scopus. Additionally, he has hands-on experience in various modeling and analysis software, including AutoCAD, Creo-3.0, Catia, Ansys, Solid Work, GEM Reservoir Simulation, Design Xpert, LISA, Google Sketchup, Matlab, etc. Dr. Kumar has also served as an editorial board member in international journals and reviewed various research papers submitted to international journals.

M. S. Munisingh research interests are in the area of development of multilayer coatings for solar thermal receiver tubes, material science and engineering, design of experiments and published 8 SCI and 4 Scopus-indexed international journals. The areas of expertise are magnetron sputtering and plasma-enhanced chemical vapor deposition techniques used to deposit metallic and hybrid/composite for absorptance, emittance, and thermal properties, stability at high temperatures for CSP applications and software tools such as COMSOL Multiphysics, CODE, TSol, and Essential Macleod simulation software to determine the absorptance and emittance and reviewer for a few international journals in material science and engineering.